Wicking in a Powder

P. S. Raux,[†,‡] H. Cockenpot,[†,‡] M. Ramaioli,[§] D. Quéré,[†,‡] and C. Clanet*,[†,‡]

[†]PMMH, UMR 7636 du CNRS, ESPCI, 75005 Paris, France
[‡]LadHyX, UMR 7646 du CNRS, Ecole Polytechnique, 91128 Palaiseau Cedex, France
[§]Department Food Science & Technology, Nestlé Research Center, 1000 Lausanne 26, Switzerland

ABSTRACT: We investigate the wicking in granular media by considering layers of grains at the surface of a liquid and discuss the critical contact angle below which spontaneous impregnation takes place. This angle is found to be on the order of 55° for monodisperse layers, significantly smaller than 90°, the threshold value for penetrating assemblies of tubes. Owing to geometry, impregnating grains is more demanding than impregnating tubes. We also consider the additional effects of polydispersity and pressure on this wetting transition and discuss the corresponding shift observed for the critical contact angle.
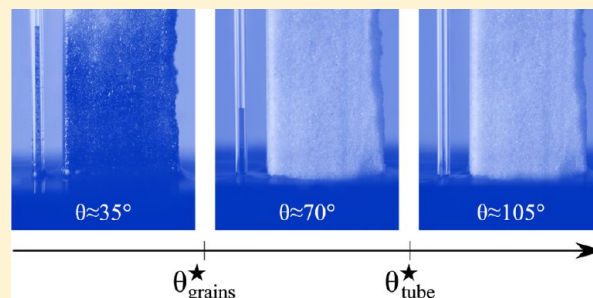
1. INTRODUCTION

The spontaneous invasion of pores by liquids is driven by a reduction in surface energy. This phenomenon is relevant to many natural applications such as soil imbibition by rain,[1−3] soil decontamination,[4] and plant physiology.[5,6] It is also of broad industrial relevance for oil extraction, civil engineering,[7] absorbent consumer goods,[8,9] paper and textile design,[10,11] and chromatographic[12] and microfluidic processes.[13] An important application in the food industry is the reconstitution of a beverage after the wetting of a dehydrated powder.[14] Depending on the field of interest, impregnation can be either beneficial (food industry) or detrimental (civil engineering).

Figure 1 compares wicking in porous media made of spherical beads and in a capillary tube. For large contact angles, there is no wicking (Figure 1a). Impregnation occurs only if the contact angle is below a critical value: 90° for the capillary tube (Figure 1b) and a much lower angle for the beads (Figure 1c). This experiment emphasizes the role of geometry in wicking: a porous medium made of grains or beads substantially differs from cylindrical capillaries because the cross-sectional area and wall orientation vary along the pores. This modifies the condition of wicking, as also shown for other special porous media such as wedges[15] and microtextures on solid surfaces.[16,17] However, the classical theories for cylindrical tubes[18−20] are still broadly applied to powders.

In the general case of a compact pile of grains, the maximum penetration height can be computed by appropriately adapting Jurin's theory.[16] In the same spirit, the classical kinetics of Lucas[21] and Washburn[22] can be modified by considering the effect of the variable cross section of the granular pores on the viscous dissipation, which generates the rich impregnation kinetics of layered beads.[23,24] In these works, the capillary driving force is often considered to be constant along the pore length. Reyssat et al.[24] considered, for instance, complete wetting and included an adjustable parameter in the capillary term. Fries et al.[23] assumed that spontaneous impregnation in

granular beds occurs if the contact angle of the liquid with the channels is lower than 90°, that is, the condition of pores having walls parallel to the pore axis. Tsori[25] and Czachor[26] theoretically studied the capillary penetration in channels of varying cross section, including sinusoidal capillaries. The former showed the existence of multiple equilibrium positions, and the latter predicted the existence of a critical wetting angle for capillary rise that depends on the sinusoidal wall waviness. Lago et al.[27] discussed the optimal angle for the highest capillary rise and found $\theta = 15.4°$ for compact piles of spherical grains. Bán et al.[28] and Shirtcliffe et al.[29] investigated spontaneous wicking in such piles. They predicted the existence of a critical contact angle $\theta^\star < 90°$ for wicking in this geometry and produced experimental evidence for this result. These works will be further commented on in sections 4 and 5.

In this article, we report experiments and discuss a model showing the existence of an acute contact angle above which the impregnation of a heap of grains can be blocked, as seen in Figure 1. We also discuss how this critical angle depends on the polydispersity, hydrostatic forcing, and disorder. These results can be used either to improve or to block capillary invasion, depending on the system of interest.

2. EXPERIMENTAL SETUP AND PROTOCOL

The experiment consists of depositing dry silanized grains of glass on the surface of a liquid bath filling a centimetric transparent cell (Figure 2a). The liquid−grain interface is observed with a camera, magnification ×2. Our wicking criterion is the detachment of grains from the interface, which then fall in the bath because of a density $\rho_s = 2450$ kg/m³ greater than that of water. Conversely, the liquid does not penetrate the pile if all the grains remain on the surface.
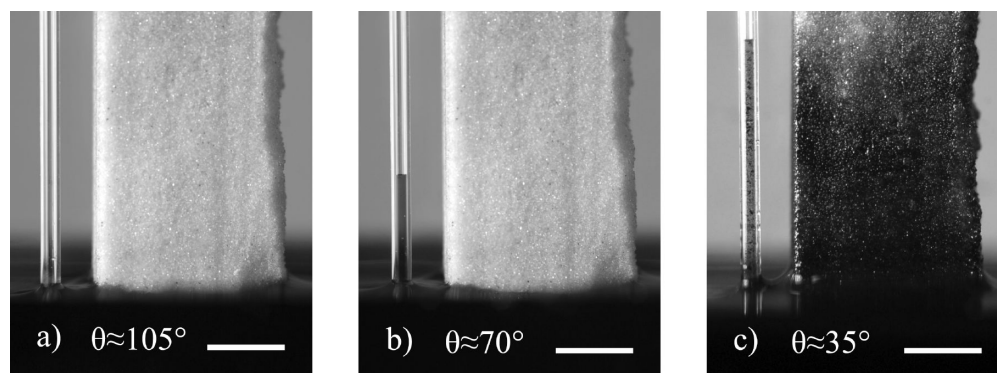
Figure 1. Silanized capillary tube and porous medium made of silanized glass beads placed in contact with various water−ethanol baths, changing the contact angle θ. (a) No wicking is observed at high contact angles. (b) Wicking in the tube occurs when the contact angle is below 90° but the grains can remain dry. (c) Spontaneous impregnation in the porous media is observed only below a critical contact angle $\theta^\star$ that is significantly smaller than 90°. Scale bars correspond to 5 mm.
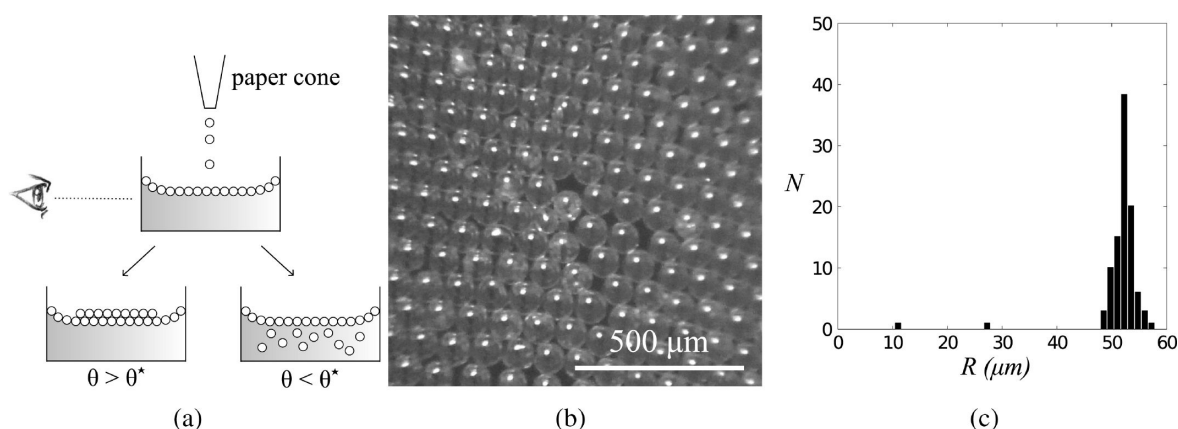

Figure 2. (a) Experimental setup and sketch of the wicking criterion. (b) Silanized glass beads of radius $R_1 = 52 \pm 2 \ \mu$m on the surface of a water−ethanol bath. (c) Corresponding distribution of bead radii for a sample of 100 beads.

The grains are borosilicate glass beads (from Sigmund Lindner) that are sieved in order to reduce the polydispersity (Figure 2b,c). Several radii R are used: 25 ± 2, 52 ± 2, 100 ± 5, and $256 \pm 13 \ \mu$m. The glass beads, initially hydrophilic, are silanized with 1H,1H,2H,2H-perfluoro-octyltriethoxysilane to be hydrophobic, following the protocol for fluorination by Qian et al.[30] The wetting properties of the system are tuned by using mixtures of water and ethanol. The ethanol volume fraction v_f in water is controlled by measuring the density of the mixture, referring to tables in ref 31. The capillary length $a = (\gamma/\rho g)^{1/2}$ (where γ and ρ are the surface tension and density of the liquid, and g is the gravity constant) varies from 2.7 mm for deionized water to 1.7 mm for pure ethanol and is always larger than the bead radius.

To measure the contact angle θ, single beads (with $R \ll a$) are placed at the surface of the liquid, and θ is deduced from the distance $\delta = R \cos \theta$ between the bead center and the liquid interface (inset in Figure 3). Pictures are taken with a Ricoh GX200 camera through binoculars at ×20. The position of the liquid−gas interface is determined by the reflection of the beads on the surface. The contact angle measurement for each v_f is repeated on 10 different beads. The contact angle θ with deionized water ($v_f = 0$) is $105 \pm 5°$, and it decreases to $35 \pm 5°$ for pure ethanol ($v_f = 1$). As reported in Figure 3, water−ethanol mixtures allow us to obtain intermediate angles, which continuously decrease from 105 to 35° as v_f passes from 0 to 1.

3. EXPERIMENTAL RESULTS

We deposit a uniform layer of dry grains on the surface of a bath of ethanol fraction v_f (Figure 4). A meniscus forms along the cell walls, which generates the dark zone observed in the figure. The actual thickness of the powder represents only a few layers of beads (typically four). Two regimes are observed. In Figure 4a, no beads fall into the
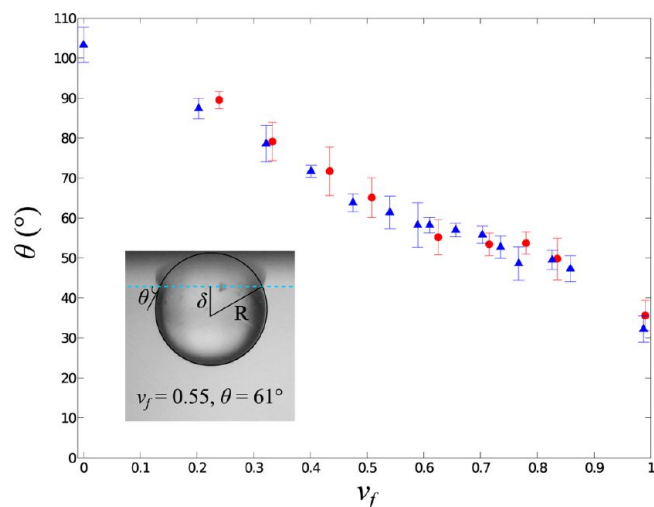

Figure 3. Contact angle θ between silanized glass beads of radius $R = 52 \ \mu$m (red circles) or $R = 256 \ \mu$m (blue triangles) and water−ethanol mixtures as a function of the ethanol volume fraction v_f. The contact angle can be continuously varied between $105 \pm 5°$ and $35 \pm 5°$ by increasing the ethanol fraction. The inset shows a typical measurement of the contact angle on a bead (with $R = 256 \ \mu$m and $v_f = 0.55$). The dashed line indicates the liquid−air interface.

bath, and the pile remains dry. In Figure 4c, beads detach and fall as the liquid invades the pile. Figure 4b shows the limit of impregnation,
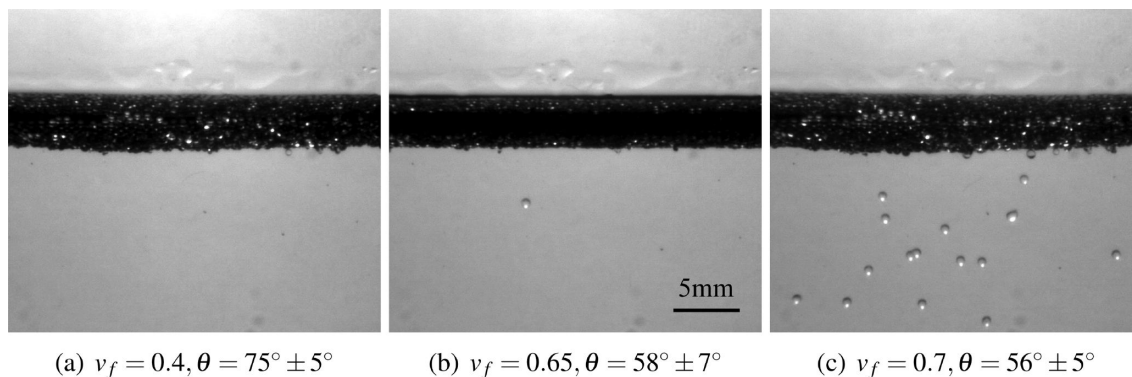
| (a) $v_f = 0.4, \theta = 75° \pm 5°$ | (b) $v_f = 0.65, \theta = 58° \pm 7°$ | (c) $v_f = 0.7, \theta = 56° \pm 5°$ |

Figure 4. Side views of our experiment for different ethanol volume fractions v_f. A pile of grains is deposited at the interface between the bath and air. The apparent thickness (in black) of the interface comes from the menisci at the edges. Wicking is deduced from the presence of grains falling into the bath: (a) no impregnation, (b) limiting case, and (c) impregnation. The glass bead radius here is 256 ± 13 μm.

where only very few beads fall. The wicking transition occurs for an ethanol fraction of $v_f^\star = 0.65 \pm 0.03$ (for $R = 256$ μm), which corresponds to a contact angle of $\theta^\star = 58 \pm 7°$. $\theta^\star$ is a critical angle: if we have $\theta < \theta^\star$, then wicking is observed; if not, then the pile remains dry. The results for different grain radii are presented in Table 1, showing that $\theta^\star$ hardly depends on R for grains smaller than the capillary length ($R \ll a$). The highest value of the critical contact angle corresponds to the largest radius. Because the density ρ_s of the grain is significantly larger than the density of the liquid, gravitational corrections are expected for the experiments with $R = 256$ μm.

Table 1. Wicking Transition in Terms of the Critical Ethanol Fraction $\nu_f^\star$ and Corresponding Contact Angle $\theta^\star$ for Different Beads of Radius R Smaller than the Capillary Length a

R (μm)	$\nu_f^\star$	$\theta^\star$ (deg)
25 ± 2	0.73 ± 0.01	53 ± 6
52 ± 2	0.73 ± 0.01	53 ± 6
100 ± 5	0.70 ± 0.01	55 ± 6
256 ± 13	0.65 ± 0.03	58 ± 7

4. MODEL

4.1. Interface Equilibrium. To explain these experiments, we first consider a single grain at the interface: because the spheres are denser than the liquid, gravity is balanced by interfacial forces. Let γ be the surface tension of the liquid; ψ, the angle between the equatorial plane and the radius that connects to the contact line; R_c, the curvature of the interface; and βR_c, the length of the liquid−air interface between the bead and the flat bath (Figure 5a). On a small scale, the angle between the sphere and the interface must be θ. All of these angles are linked by the geometrical relationship

$$\psi + \theta - \beta = \frac{\pi}{2} \tag{1}$$

Keller[32] has shown that the vertical projection of the pressure forces is equal to the weight of the volume of liquid bounded by the horizontal free surface of the bath, the wetted surface of the body, and the vertical cylinder of radius $R \cos \psi$ and height $\xi = R_c(1 - \cos \beta)$ (in white below the dashed line in Figure 5a). At equilibrium, the vertical projection of forces on the body can be written as a balance between the surface force $2\pi R \gamma \cos\psi \sin\beta$ (corresponding to the weight of the volume in gray in Figure 5a) and an effective weight $4/3\pi R^3 g\rho_{eff}$, gathering the buoyancy and the weight of the sphere. This leads to
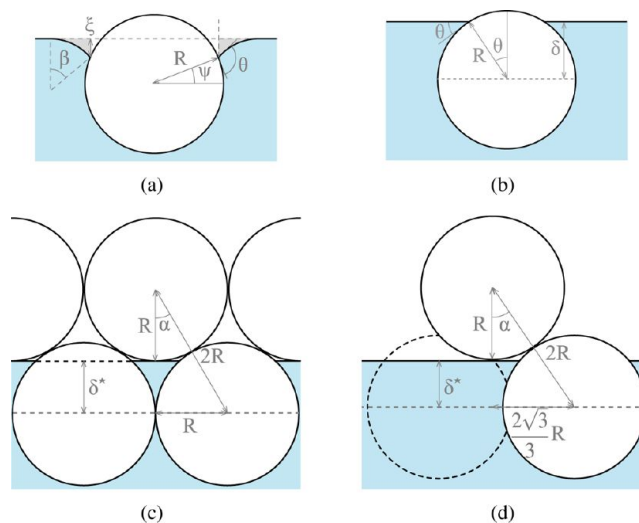

Figure 5. (a) Sphere at a curved interface. (b) Equilibrium state of a small bead at a liquid−gas interface. (c) Limiting case for the impregnation in 2-D close packing: the interface is tangent to the upper spheres. (d) Projection along the plane given by a median of the base of the tetrahedron and its summit for a 3-D pile. The dashed circle represents the two other spheres forming the base of the tetrahedron, out of the plane of the figure.

$$\sin \beta = \frac{2R^2 g \rho_{eff}}{3\gamma \cos \psi} = \frac{\rho_{eff}}{\rho} \frac{R^2}{a^2} \frac{2}{3 \cos \psi} \tag{2}$$

where $a = (\gamma/\rho g)^{1/2}$ is the capillary length. In our case, the radii are much smaller than the capillary length, and the ratio of densities is of order unity. Thus, $\sin \beta$ is small, on the order of 10^{-2} for $R \approx 100$ μm. For $\theta > 0$, we can neglect the effect of the weight and consider a flat interface as indeed observed in the experiments (inset in Figure 3). This corresponds to $\psi + \theta = \pi/2$. The sphere equator stabilizes at a height δ below the flat interface (Figure 5b), where δ is given by

$$\delta = R \cos \theta \tag{3}$$

4.2. Two-Dimensional Pile. On the basis of the experimental observation in Figure 2b, we consider a compact pile of grains (Figure 5c). As the equilibrium previously discussed is achieved for the first layer, the liquid may reach the second layer of grains. If it happens, the contact line is no longer at equilibrium and it will move up into the pile until it satisfies both a flat interface and a contact angle θ on the

second layer. As it did for the first layer, it reaches the next spheres, and the same mechanism applies: no equilibrium is possible as long as there are dry grains. Liquid impregnates the pile, until the last monolayer of grains gets trapped at the interface. As the liquid rises, lower spheres become surrounded by liquid and thus detach from the rest of the pile and fall into the bath, as seen in Figure 4c. Conversely, if the liquid does not reach the second layer of grains, only the first layer contacts the liquid and no grain detaches from the interface.

The limit between these two situations corresponds to $\theta = \theta_{2D}^\star$, for which the interface is tangent to the spheres of the second layer (Figure 5c). The distance between two equatorial planes is $R + \delta^\star$, which can also be written by introducing the angle α between the line linking the centers of the sphere from different layers with the normal to the first layer (Figure 5c):

$$R + \delta^\star = 2R \cos \alpha \tag{4}$$

In the compact 2-D case, the centers of monodisperse grains form equilateral triangles, which yield $\alpha = 30°$. Together with eqs 3 and 4, this provides the value of the critical contact angle $\theta_{2D}^\star$ for impregnating a 2-D pile (assembly of infinite cylinders):

$$\theta_{2D}^\star = \arccos(\sqrt{3} - 1) \approx 43° \tag{5}$$

If the contact angle θ is larger than this critical value (and smaller than 90°), there is a local minimum in the surface energy of the system: impregnation can be blocked. The system may not reach its global energy minimum, owing to the existence of an energy barrier ΔE (per unit length) given by

$$\frac{\Delta E}{2\pi R \gamma} = \frac{\sin \theta - \sin \theta^\star + (\theta^\star - \theta)\cos \theta}{\pi} \tag{6}$$

This expression becomes, at leading order in $\theta - \theta^\star$,

$$\frac{\Delta E}{2\pi R \gamma} = \frac{\sin \theta^\star}{2\pi}(\theta - \theta^\star)^2 \tag{7}$$

For a bead diameter of $2R \approx 100 \ \mu m$, the magnitude of the energy barrier typically is $2R\Delta E \approx 10^{-12}$ J, which is of course much larger than the thermal energy.

4.3. Three-Dimensional Geometry. Similar effects are expected in 3-D, and Shirtcliffe et al.[29] used surface free energies to predict the existence of a critical contact angle of wicking of 50.73° for a compact pile. We can also obtain this result using geometrical considerations. In a 3-D compact pile of spheres, the grains form a tetrahedral network. The discussion above is still correct as well as eqs 3 and 4, but the relative position of the successive layers is slightly modified, leading to a different value of α, now given by $\sin \alpha = 3^{1/2}/3$ (Figure 5d). This provides the critical angle for impregnating a 3-D pile, as also proposed by Bán et al.[28] and Shirtcliffe et al.:[29]

$$\theta_0^\star = \arccos\left(\sqrt{\frac{8}{3}} - 1\right) \approx 51° \tag{8}$$

In our experiments, in contrast to previous approaches,[28,29] we measure the contact angle directly on the grains, as discussed in section 1. Moreover, we bring the grains into contact with the liquid without confinement. Using this experimental protocol allows us to detect impregnation as it occurs over a single grain layer, improving the precision of the measurement. The observed critical contact angles (Table 1) are indeed close to $\theta_0^\star \approx 51°$ yet slightly larger. (An additional deviation appears when R is greater than 100 μm, revealing the

influence of gravity, which is neglected in the model.) A different hypothesis can be proposed to explain this small (yet systematic) difference. (1) Experimentally, wicking is reported as soon as the first grain detaches. Thus if the actual critical contact angle $\theta^\star$ locally differs from $\theta_0^\star$, our experimental criterion will determine only the highest possible critical contact angle. (2) In Figure 2c, one can see that the diameter of the grains is not perfectly fixed, corresponding to the standard deviations reported in Table 1. A small polydispersity can modify the geometry inside the pile so that the local value of the critical angle $\theta^\star$ can be different from the monodisperse value, $\theta_0^\star$. In section 4, we investigate an elementary case of polydispersity—two differently sized piles. (3) The interface was supposed to be flat, which is not the case if the difference in pressure through the interface is not negligible. In section 5, we discuss the effect of pressure for a pile of thickness comparable to the capillary length. (4) The determination of $\theta_0^\star$ assumes a close packing of spherical particles. As discussed in section 6, if the compactness of the pile is lower or if the particles are slightly elongated, then defects in the pile can appear, modifying the wetting transition.

5. POLYDISPERSITY

As observed in Figure 2c, there is a small dispersion of bead radii. Bán et al. considered a polydisperse packing and anticipated theoretically that impregnation should be easier ($\theta^\star$ should be larger) than in a monodisperse pile, although they found no difference experimentally.[28]

The theoretical determination of the critical angle is similar to the monodisperse case in three dimensions, but the geometry is modified by the bidispersity of the grains (Figure 6). Equation 3 can now be written for the lower layer:

$$\delta = R_1 \cos \theta \tag{9}$$

In addition, we have

$$R_2 + \delta = (R_1 + R_2)\cos \alpha \tag{10}$$

where α is determined by

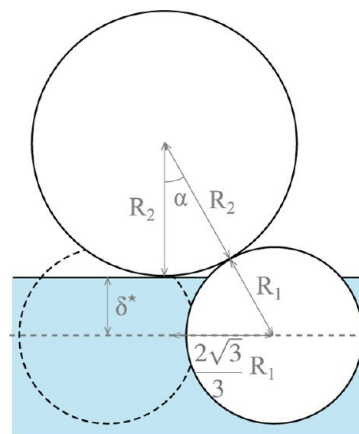$$\sin \alpha = \frac{2}{\sqrt{3}} \frac{R_1}{R_1 + R_2} \tag{11}$$

Figure 6. Limiting case of impregnation for a bilayer of bidisperse grains. The dashed circle represents the spheres of the lower layer out of the plane of the projection.
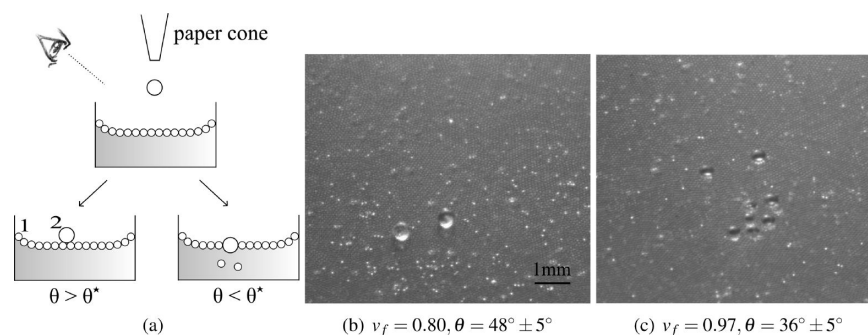
Figure 7. (a) Setup of the bidisperse experiment. (b) $R_2 = 256 \pm 13\ \mu$m beads stay on top of the base monolayer of radius $R_1 = 52 \pm 2\ \mu$m. (c) The same experiment, with a lower contact angle ($\theta < \theta^\star$). The R_2 spheres partially pass through the monolayer, and only their top poles remain visible.

Using eqs 9−11, we obtain the critical angle $\theta^\star$ as a function of the ratio $r = R_1/R_2$ (<1):

$$\cos\theta^\star = \frac{\sqrt{1 + 2r - \frac{r^2}{3}} - 1}{r} \qquad (12)$$

If the upper spheres are much larger than the lower ones ($r \rightarrow 0$), then the critical contact angle goes to 0°. Interestingly, this equation remains the same if the upper beads are the small ones ($r > 1$), and it is valid as long as the upper spheres are large enough to stand on the lower layer, that is, $r < 3 + 2(3^{1/2})$. In the monodisperse limit ($r \rightarrow 1$), eq 12 gives the same result as eq 8. Additionally, for a small polydispersity, it yields, to leading order in $(r - 1)$,

$$\cos\theta^\star = \cos\theta_0^\star + \left(1 - \frac{\sqrt{6}}{2}\right)(r - 1) \qquad (13)$$

Because $1 - 6^{1/2}/2$ is negative, $\theta^\star$ increases with r and exceeds $\theta_0^\star$ for small spheres on large ones ($r > 1$). This situation is favorable to wicking and thus should determine the path that is followed during the wicking of a random bidisperse pile. Therefore, for applications where wicking has to be guaranteed or prevented, eq 12 allows us to identify the most stringent contact angle condition, which has to be met in the most unfavorable case of local segregation.

To investigate experimentally the effect of polydispersity, we achieved two layer systems, with each one being formed from beads of a given size. Combinations of spheres presented in Table 1 were used to obtain values of r between 0.2 and 2.5. A monolayer of beads of radius R_1 is first placed at the surface of the bath with a contact angle θ. Then beads of radius R_2 are added one by one (Figure 7a). We observe two regimes, depending on θ. If $\theta > \theta^\star$, then the beads of radius R_2 stay on the monolayer of beads of radius R_1, and no impregnation is observed (Figure 7b). In contrast, for $\theta < \theta^\star$, beads of radius R_2 are wetted and pass partially through the interface between the beads of the monolayer (Figure 7c). Some R_1 beads detach from the interface and sink into the liquid whereas only the north pole of the upper sphere remains dry. The measured critical angle $\theta^\star$ is very sensitive to the polydispersity of these elementary piles because it varies from $\theta^\star = 36°$ for $r = 0.2$ to $\theta^\star = 62°$ for $r = 2$, as reported in Figure 8. Equation 12 is coherent with the data, even if the value of the critical contact angle seems to be slightly underestimated (Figure 8). This discrepancy may be due to defects in the packing of the base monolayer, which is investigated in section 6. However, this
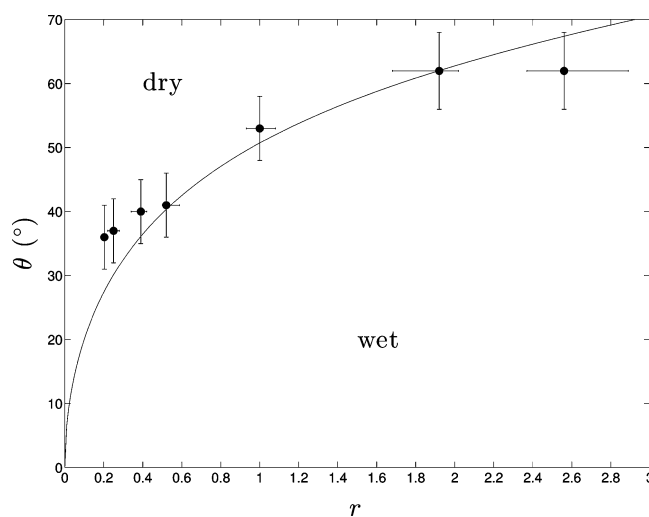

Figure 8. Wicking phase diagram for a bidisperse powder in terms of the contact angle θ versus the ratio of grain radii $r = R_1/R_2$. Dots are data for the critical angle $\theta^\star$, and the solid line is eq 12. It is found that the smaller the r value, the easier the wicking.

experiment emphasizes again how critical the geometry is in the wicking of grains.

Coming back to the monodisperse experiments of section 1, the size of the beads slightly varies from one layer to another, hence modifying the local critical contact angle. The dispersion of the radius typically yields $r \approx 1.1$ (Table 1), which generates a critical angle $\theta^\star$ of 52°: polydispersity can explain part of the difference between the experimental data in Table 1 and the theoretical value of $\theta_0^\star$ expected from eq 8.

6. HYDROSTATIC FORCING

Even if the thickness h of the dry pile was set to be as small as possible in section 2, spheres can be coarse enough to make h comparable to the capillary length a. In this case, the hydrostatic pressure plays a role, changing the shape of the interface between beads and thus the limit for impregnation. The experiment in Figure 9 shows the influence of the pile thickness on wicking. On a liquid with a contact angle of $\theta > \theta_0^\star$ (no wicking), we locally feed the surface with beads to increase the thickness. For h lower than a threshold $h^\star$, the pile remains dry (Figure 9a). As the thickness h reaches $h^\star$, a few grains detach from the interface (Figure 9b). For thicker piles, the dry powder is impregnated, and many beads fall into the bath (Figure 9c). The reference $h = 0$ is taken at the lowest point of the meniscus in the transparent cell, before any grains are
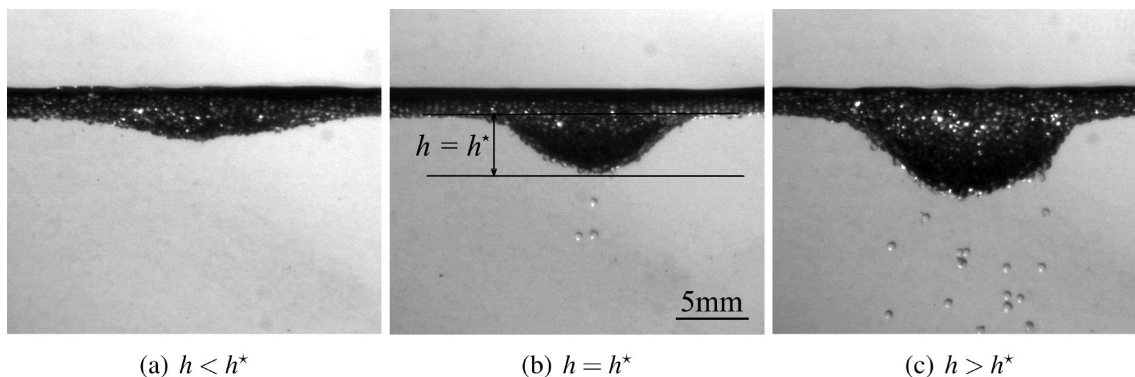
(a) $h < h^\star$ (b) $h = h^\star$ (c) $h > h^\star$

Figure 9. Forced impregnation at an ethanol volume fraction of $v_f = 0.33$ with varying pile thickness h. The contact angle here is $\theta = 80° \pm 5° > \theta_0^\star$. When h is greater than $h^\star$, impregnation is observed.
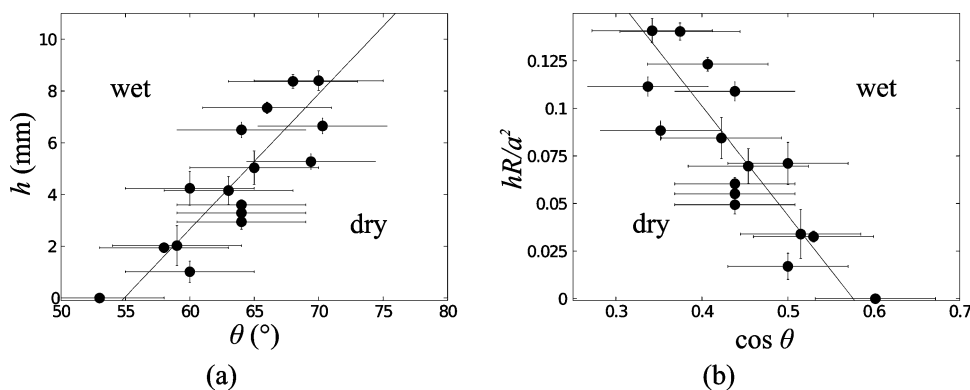

Figure 10. (a) Phase diagram for the thickness h of the pile as a function of the contact angle θ. The dots correspond to the limit between wet and dry states and thus represent the critical thickness $h^\star$ of wicking for beads of radius $R = 52$ μm. The line is a linear regression of slope 30 mm/rad. (b) Phase diagram in terms of the normalized thickness of powder and the cosine of the contact angle (for $R = 52$ μm).

added. Figure 10a shows a phase diagram (θ, h) separating dry and wet states. At a given height h, wicking occurs only if θ is smaller than a critical value $\theta^\star$, which increases with h. The two domains are separated by a line of slope 30 mm/rad for $R = 52$ μm.

If the grain radius is comparable to a or if there is a pressure difference ΔP between the liquid and the gas, then the interface is curved between the beads, as illustrated in Figure 11. The associated Laplace pressure compensates for the pressure ΔP and changes the condition for impregnation. The Laplace equation gives the radius of curvature of the meniscus at equilibrium $(\gamma/\Delta P)$, where γ is the surface tension of the liquid.
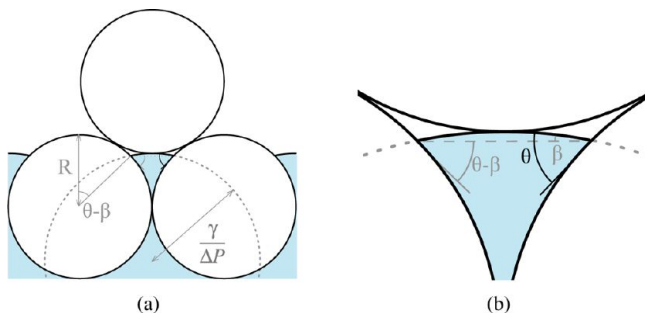

Figure 11. Limit of impregnation with forcing and close up of the meniscus. Because of the curvature of the meniscus, the liquid reaches the second layer of grains, and no impregnation would have been observed with a flat meniscus and the same contact angle.

The sign of this curvature is related to the sign of the forcing: a larger pressure in the liquid helps the impregnation process, elevating the highest point of the meniscus (Figure 11). The expression for δ changes, but eq 4 remains correct. If β is the angle between the meniscus at the contact point with the sphere and the equatorial plane (Figure 11), we can write

$$\delta = R \cos(\theta - \beta) + \frac{\gamma}{\Delta P}(1 - \cos\beta) \tag{14}$$

The distance between the two contact points can be written as a function of either β or $\theta - \beta$ (Figure 11), which leads to

$$\frac{\gamma}{\Delta P} \sin\beta = R(1 - \sin(\theta - \beta)) \tag{15}$$

To determine β, we can consider a situation close to the flat meniscus. Assuming $\beta \ll 1$ and a meniscus radius larger than the grain diameter $(R\Delta P/\gamma \ll 1)$, eq 15 simplifies at leading order to

$$\beta = \frac{R\Delta P}{\gamma}(1 - \sin\theta) \tag{16}$$

Hence eq 14 becomes

$$\delta = R \cos\theta + \frac{R^2 \Delta P}{2\gamma} \cos^2\theta \tag{17}$$

As shown in section 3, the critical angle for impregnation with a flat meniscus is given by $\cos\theta_0^\star = \delta/R$. With a curved meniscus, the critical contact angle $\theta^\star$ is the angle θ obtained from solving eq 17, which yields for leading order

(a) $\theta = 105°$, $R = 52\ \mu m$ (b) $\theta = 105°$, $R = 100\ \mu m$ (c) $\theta = 45°$, $R = 52\ \mu m$ (d) $\theta = 45°$, $R = 100\ \mu m$
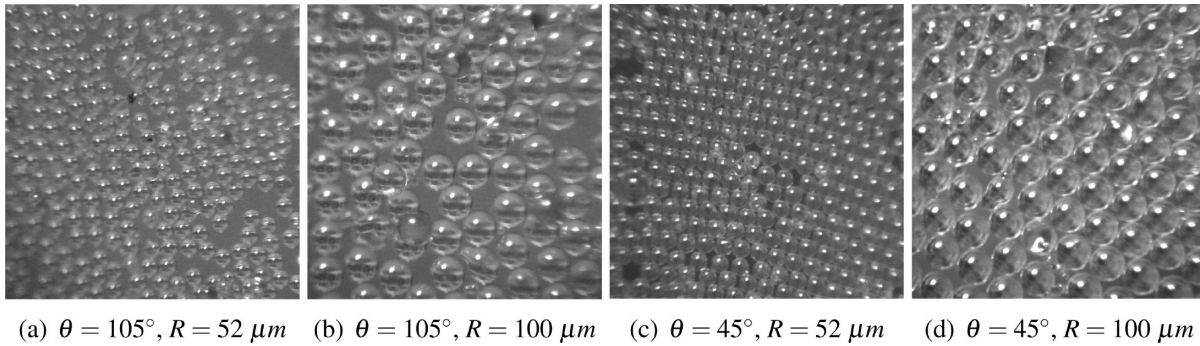
Figure 12. Compactness of monolayers of grains of radius R and contact angle θ at the surface of water−ethanol solutions. The pictures are taken from above through binoculars at ×20 magnification.
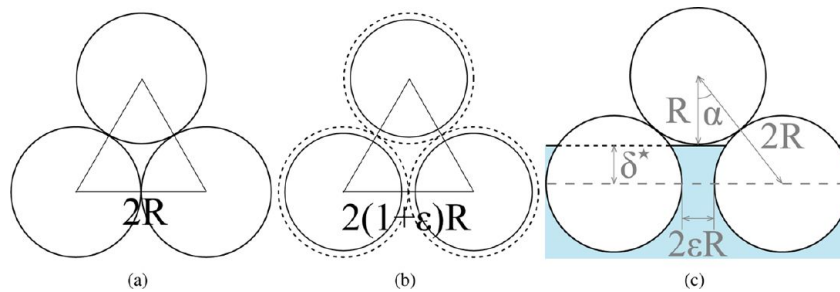

Figure 13. Surface fraction occupied by spheres at the liquid−air interface: in the triangle, the surface of the grains is $\pi R^2/2$. In the close-packing case (a), the total surface is $3^{1/2}R^2$ whereas it is $3^{1/2}(1 + \varepsilon)^2 R^2$ if there is a gap $2\varepsilon R$ between spheres (b). As model defects in the first layer of the pile, we consider gaps $2\varepsilon R$ between the grains (c).

$$\cos \theta^\star = \cos \theta_0^\star - \frac{R\Delta P}{2\gamma} \cos^2 \theta_0^\star \tag{18}$$

If the pressure ΔP is negative, which means a higher pressure in air, then it is harder to impregnate the pile ($\theta^\star < \theta_0^\star$): the liquid has to wet more of the surface to wet the grains. Conversely, if the pressure is positive, then a liquid with θ larger than $\theta_0^\star$ can invade the pile. If the grain radius is comparable to the capillary length, then the curvature is set by the balance among the weight of the sphere, the buoyancy, and the surface tension. Its sign will depend on the balance of the first two forces: if the spheres are denser than the liquid, then the curvature is positive and piles of such spheres can be impregnated at a contact angle higher than $\theta_0^\star$, as indeed observed with the largest beads in Table 1.

As seen in Figure 9, the pressure can be imposed hydrostatically: we have $\Delta P = \rho g h$, where h is the depth of the deepest point of the pile (Figure 9b). According to eq 18, the cosine of the critical contact angle should be linear in h. A liquid with a contact angle of $\theta > \theta_0^\star$ invades the powder if h is higher than a critical value $h^\star$ given by

$$h^\star = \frac{2a^2}{R} \frac{\cos \theta_0^\star - \cos \theta}{\cos^2 \theta_0^\star} \tag{19}$$

where $\cos \theta_0^\star = (^8/_3)^{1/2} - 1$ (eq 8) and $a^2 \approx 3.1 \pm 0.1$ mm^2 (a quantity almost constant in the tested range of the ethanol volume fraction). In Figure 10b, the normalized critical height $h^\star$ is observed to decrease as $\cos \theta$ increases, as predicted by eq 19. However, the experimental value of the slope is −0.6, which is 1 order of magnitude smaller than the slope predicted by our model, $-2/\cos^2 \theta_0^\star \approx -5$. This discrepancy might be due to large errors in both $h^\star$ and the contact angle, measured in a narrow domain of $\cos \theta$.

7. ECCENTRICITY AND DEFECTS IN THE PILE

Defects in the packing of the pile may also affect impregnation. Indeed, the observation of a monolayer of beads (Figure 12) shows deviations from close packing. The packing depends on the way that the monolayer is prepared, and defects especially occur if the liquid does not impregnate a monodisperse pile ($\theta > \theta^\star$). In this section, we consider as a model defect gaps between spheres. Typical values for the gap are obtained by comparing the surface fraction occupied by the spheres to a compact situation. In 2-D close packing, the surface fraction occupied by spheres is $\Phi_c = \pi/2(3^{1/2})$ (Figure 13a). If the spheres have a gap of $2\varepsilon R$ between them, then the compaction decreases to $\Phi = \Phi_c/(1 + \varepsilon)^2$ (Figure 13b), so the dimensionless gap can be expressed as

$$\varepsilon = \sqrt{\frac{\Phi_c}{\Phi}} - 1. \tag{20}$$

From pictures such as those shown in Figure 12, we can extract the compacness Φ and thus deduce a mean value for ε, as reported in Table 2. Experimentally, the monolayer has fewer defects when made on a wicking liquid for a monodisperse pile: a small excess of grains will be removed by the wicking of the pile, as described earlier (section 3), leaving only a compact

Table 2. Estimated Values of the Surface Fraction of Beads Φ and Average Relative Gap ε Corresponding to the Different Situations and Radii

R (μm)	$\theta = 45° < \theta^\star$	$\theta = 105° > \theta^\star$
52 ± 2	$\Phi = 0.90$, $\varepsilon = 0.4\%$	$\Phi = 0.72$, $\varepsilon = 12\%$
100 ± 5	$\Phi = 0.87$, $\varepsilon = 2.1\%$	$\Phi = 0.76$, $\varepsilon = 9.2\%$
256 ± 13	$\Phi = 0.86$, $\varepsilon = 2.7\%$	$\Phi = 0.82$, $\varepsilon = 5.2\%$

monolayer. In the polydisperse case and for $r > 1$, we are in the opposite situation and thus expect the base monolayer to be poorly packed.

We focus on the situation favoring wicking, in particular, when a defect is present in the first layer of grains (Figure 13c). For a monodisperse pile, eqs 3 and 4 are still correct. In the 3-D case, because the base of the tetrahedron is loose, as sketched in Figure 13b, α is given by $\sin \alpha = 3^{1/2}/3(1 + \varepsilon)$. These equations lead to a modified critical angle function of ε,

$$\cos \theta^{\star} = \sqrt{\frac{8}{3}\left(1 - \varepsilon - \frac{\varepsilon^2}{2}\right)} - 1 \tag{21}$$

which becomes, for low ε,

$$\cos \theta^{\star} = \cos \theta_0^{\star} - \sqrt{\frac{2}{3}}\,\varepsilon \tag{22}$$

These equations show that introducing defects into the packing ($\varepsilon > 0$) tends to increase $\theta^{\star}$ so that wicking becomes less demanding in terms of the contact angle, thus approaching the classical assumption of $\theta^{\star} = 90°$. Applying eq 22 to the experimental values of Table 1 leads to estimations of ε in the monodisperse case: we find that $\varepsilon = 4\%$ for $R = 25$ and $52\ \mu m$, $\varepsilon = 7\%$ for $R = 100\ \mu m$, and $\varepsilon = 13\%$ for $R = 256\ \mu m$. These results are coherent with the fact that smaller spheres form more compact layers because of the relatively stronger interaction of the meniscus (Figure 12c,d).[33] These estimations are, however, slightly higher than observed on monolayers (Table 2), but the latter values are average quantitites whereas the experimental protocol is sensitive to larger local values of ε.

8. CONCLUSIONS

To study the wicking in granular media, we carried out experiments on piles of glass beads at the surface of a bath and showed the existence of a critical angle $\theta^{\star}$ below which wicking occurs. This angle is significantly smaller than that observed in capillary tubes (90°), and its value is close to the value expected from models, around 51°. This critical angle can be modified by a pressure gradient across the liquid–air interface, defects in the pile compacity, or the polydispersity of the grains. These effects can be used in industrial processes to either help or prevent the wicking of a powder, depending on the field of application. Moreover, this study emphasizes the crucial role of geometry in the wicking of ordered powders. More generally, the geometry of porous media allows one to control the penetration or to prevent the invasion of this medium by a given liquid, which permits a wetting liquid to be repelled from a solid surface, as observed with superoleophobic materials.[34]

■ AUTHOR INFORMATION

Notes

The authors declare no competing financial interest.

■ REFERENCES

(1) Green, W. H.; Ampt, G. A. Studies on Soil Physics. *J. Agric. Sci.* **1911**, *4*, 1–24.

(2) Doerr, S. H.; Shakesby, R. A.; Walsh, R. P. D. Soil Water Repellency: Its Causes, Characteristics and Hydro-Geomorphological Significance. *Earth Sci. Rev.* **2000**, *51*, 33–65.

(3) Doerr, S. H.; Shakesby, R. A.; Dekker, L. W.; Ritsema, C. J. Occurrence, Prediction and Hydrological Effects of Water Repellency Amongst Major Soil and Land-Use Types in a Humid Temperate Climate. *Eur. J. Soil Sci.* **2006**, *57*, 741–754.

(4) Amro, M. M. Factors Affecting Chemical Remediation of Oil Contaminated Water-Wetted Soil. *Chem. Eng. Technol.* **2004**, *27*, 890–894.

(5) Taiz, L.; Zeiger, E. *Plant Physiology*; Sinauer: Sunderland, 1998.

(6) Ponomarenko, A.; Quéré, D.; Clanet, C. A Universal Law for Capillary Rise in Corners. *J. Fluid Mech.* **2011**, *666*, 146–154.

(7) Hall, C.; Hoff, W. D. *Water Transport in Brick, Stone and Concrete*, 2nd ed.; Spon Press: London, 2002.

(8) Staples, T. L.; Shaffer, D. G. Wicking Flow in Irregular Capillaries. *Colloids Surf., A* **2002**, *204*, 239–250.

(9) Brielles, N.; Chantraine, F.; Viana, M.; Chulia, D.; Branlard, P.; Rubinstenn, G.; Lequeux, F.; Mondain-Monval, O. Dissolution of a Surfactant-Containing Active Porous Material. *J. Colloid Interface Sci.* **2008**, *328*, 344–352.

(10) Bico, J.; Quéré, D. Precursors of Impregnation. *Europhys. Lett.* **2007**, *61*, 348–353.

(11) Alava, M.; Niskanen, K. The Physics of Paper. *Rep. Prog. Phys.* **2006**, *69*, 669–723.

(12) Wall, P. E. *Thin Layer Chromatography: A Modern Practical Approach*; Royal Society of Chemistry: London, 2005.

(13) Bouaidat, S.; Hansen, O.; Bruus, H.; Berendsen, C.; Bau-Madsen, N. K.; Thomsen, P.; Wolff, A.; Jonsmann, J. Surface-Directed Capillary System; Theory, Experiments and Applications. *Lab Chip* **2005**, *5*, 827–836.

(14) Forny, L.; Marabi, A.; Palzer, S. Wetting, Disintegration and Dissolution of Agglomerated Water Soluble Powders. *Powder Technol.* **2011**, *206*, 72–78.

(15) Concus, P.; Finn, R. On the behavior of a capillary surface in a wedge. *Proc. Natl. Acad. Sci. U.S.A.* **1969**, *63*, 292–299.

(16) de Gennes, P.-G.; Brochard-Wyart, F.; Quéré, D. *Capillarity and Wetting Phenomena: Drops, Bubbles, Pearls, Waves*; Springer: New York, 2004.

(17) Blow, M. L.; Kusumaatmaja, H.; Yeomans, J. M. Imbibition through an Array of Triangular Posts. *J. Phys.: Condens. Matter* **2009**, *21*, 464125.

(18) Hauksbee, F. R. S. Several Experiments Touching the Seeming Spontaneous Ascent of Water. *Philos. Trans. R. Soc. London* **1708/1709**, *26*, 258–266.

(19) Jurin, J. An Account of Some Experiments Shown before the Royal Society; With an Enquiry into the Cause of the Ascent and Suspension of Water in Capillary. *Philos. Trans. R. Soc. London* **1717/1719**, *30*, 739–747.

(20) Laplace, P. S. *Theory of Capillary Attraction. Supplements to the 10th book of Celestial Mechanics*, 1806/1807; Reprinted by Chelsea: New York, 1966.

(21) Lucas, R. Ueber das Zeitgesetz des Kapillaren Aufstiegs von Flüssigkeiten. *Kolloid Z. Z. Polym.* **1918**, *23*, 15–22.

(22) Washburn, E. W. The Dynamics of Capillary Flow. *Phys. Rev.* **1921**, *17*, 273–283.

(23) Fries, N.; Dreyer, M. An Analytic Solution of Capillary Rise Restrained by Gravity. *J. Colloid Interface Sci.* **2008**, *320*, 259–263.

(24) Reyssat, M.; Sangne, L. Y.; van Nierop, E. A.; Stone, H. A. Imbibition in Layered Systems of Packed Beads. *Europhys. Lett.* **2009**, *86*, 56002.

(25) Tsori, Y. Discontinuous Liquid Rise in Capillaries with Varying Cross-Sections. *Langmuir* **2006**, *22*, 8860–8863.

(26) Czachor, H. Modelling the Effect of Pore Structure and Wetting Angles on Capillary Rise in Soils Having Different Wettabilities. *J. Hydrol.* **2006**, *328*, 604–613.

(27) Lago, M.; Araujo, M. Capillary Rise in Porous Media. *Phys. A* **2001**, *289*, 1–17.

(28) Bán, S.; Wolfram, E.; Rohrsetzer, S. The Condition of Starting of Liquid Imbibition in Powders. *Colloids Surf.* **1987**, *22*, 291–300.

(29) Shirtcliffe, N. J.; McHale, G.; Newton, M. I.; Pyatt, F. B.; Doerr, S. H. Critical Conditions for the Wetting of soils. *Appl. Phys. Lett.* **2006**, *89*, 094101.

(30) Qian, B.; Shen, Z. Fabrication of Superhydrophobic Surfaces by Dislocation-Selective Chemical Etching on Aluminum, Copper, And Zinc Substrates. *Langmuir* **2005**, *21*, 9007–9009.

(31) Hodgeman, C. D. *Handbook of Chemistry and Physics*, 31st ed.; Chemical Rubber Company Publications: Cleveland, OH, 1949; pp 1693−1699.

(32) Keller, J. B. Surface Tension Force on a Partly Submerged Body. *Phys. Fluids* **1998**, *10*, 3009−3010.

(33) Mansfield, E. H.; Sepangi, H. R.; Eastwood, E. A. Equilibrium and Mutual Attraction or Repulsion of Objects Supported by Surface Tension. *Philos. Trans. R. Soc. London* **1997**, *355*, 869−919.

(34) Tuteja, A.; Choi, W.; Ma, M.; Mabry, J. M.; Mazzella, S. A.; Rutledge, G. C.; McKinley, G. H.; Cohen, R. E. Designing Superoleophobic Surfaces. *Science* **2007**, *318*, 1618−1622.